**NEURO**

Fabrice Bonneville
Julien Savatovsky
Jacques Chiras

# Imaging of cerebellopontine angle lesions: an update. Part 1: enhancing extra-axial lesions

F. Bonneville (✉) · J. Chiras
Department of Neuroradiology,
Pitié-Salpêtrière Hospital,
47, Boulevard de l'Hôpital,
75013 Paris, France
e-mail: fabrice.bonneville@psl.aphp.fr
Tel.: +33-142163596
Fax: +33-142163515

J. Savatovsky
Department of Radiology, Adolphe de
Rothschild Fondation,
Paris, France

**Abstract** Computed tomography (CT) and magnetic resonance (MR) imaging reliably demonstrate typical features of vestibular schwannomas or meningiomas in the vast majority of mass lesions in the cerebellopontine angle (CPA). However, a large variety of unusual lesions can also be encountered in the CPA. Covering the entire spectrum of lesions potentially found in the CPA, these articles explain the pertinent neuroimaging features that radiologists need to know to make clinically relevant diagnoses in these cases, including data from diffusion and perfusion-weighted imaging or MR spectroscopy, when available. A diagnostic algorithm based on the lesion's site of origin, shape and margins, density, signal intensity and contrast material uptake is also proposed. Part 1 describes the different enhancing extra-axial CPA masses primarily arising from the cerebellopontine cistern and its contents, including vestibular and non-vestibular schwannomas, meningioma, metastasis, aneurysm, tuberculosis and other miscellaneous meningeal lesions.

**Keywords** Cerebellopontine angle · Brain tumours · Magnetic resonance imaging · Diffusion imaging

## Introduction

The cerebellopontine angle (CPA) cistern is a subarachnoid space containing cranial nerves and vessels bathed in cerebrospinal fluid (CSF). The CPA is bounded by the pons, the anterior aspect of the cerebellum and the petrous temporal bone covered by dura mater. It is centred by the internal auditory canal (IAC) and extends caudally from the Vth cranial nerve to the IX-X-XIth cranial nerve complex. CPA lesions are clinically non-specific and the presenting symptoms are not related to the nature of the lesion itself, but to the nerves or cerebral structures involved with the lesions. Therefore, preoperative diagnosis of a CPA region tumour is mainly based on imaging. Diagnosis may be difficult because of the wide variety of cell types and origins of such tumours (Fig. 1) [1, 2]. Because vestibular schwannomas account for 70%–80% of all CPA lesions, meningiomas 10%–15% and epidermoid cysts 5%, the few remaining lesions, which account for less than 1% each, are derived from an extraordinarily wide spectrum of unusual lesions that are challenging to diagnose. In addition to the computed tomography (CT) and conventional magnetic resonance (MR) imaging characteristics of the different CPA lesions (including anatomic site of origin, shape, density, signal and behaviour after contrast media injection), these articles also provide data from MR advanced techniques such as diffusion-weighted imaging (DWI) and perfusion imaging, as well as MR spectroscopy, when available, as they may bring crucial new data that allow accurate preoperative diagnosis.

In this work, we initiate the approach depending on the result of a simple question: does the mass lesion enhance after contrast administration? If the answer is yes, the site of origin of the lesion is then determined as it leads to three different gamuts based on whether the mass originates within the CPA cistern itself, the cerebellum or brain stem, or the skull base. If the answer is no, then the intrinsic T1 signal intensity is crucial: it points toward a cystic lesion if low, or a lesion with fat or a high protein content if high. Based on all these specific imaging characteristics

provided for all lesions potentially encountered in the CPA, a concise algorithm is proposed to facilitate diagnosis (Fig. 1). We review in this paper only the different enhancing extra-axial lesions appearing as very focal mass lesions located in the CPA, thus excluding diffuse posterior fossa meningeal thickening, while non-enhancing extra-axial lesions as well as skull base and intra-axial lesions invading the CPA are discussed in the second part of this work.

## Enhancing extra-axial lesions originating in the CPA

Extra-axial lesions are theoretically easily recognized in the CPA: they are separated from the brain parenchyma by a cleft of cerebrospinal fluid and may enlarge the cerebellopontine cistern. They also push the cranial nerves, the brain stem or the anterior aspect of the cerebellum away.

Demonstration of vessels interposed between the mass lesion and the brain parenchyma is another sign of the extra-axial origin of the lesion. Such lesions include schwannomas and a wide spectrum of meningeal mass lesions, as well as vascular lesions.

### Vestibular schwannoma

Vestibular schwannoma (formerly called acoustic neuroma) is by far the most frequent tumour in the CPA, accounting for 70% to 80% of all CPA masses [3]. Most vestibular schwannomas develop from the Schwann sheath of the inferior vestibular nerve in the IAC where they grow slowly. Then, they smoothly erode the posterior edge of the porus acusticus and may give rise to a round or oval component in the CPA cistern, thus giving the typical "ice cream on cone" pattern. At CT, schwannomas are usually
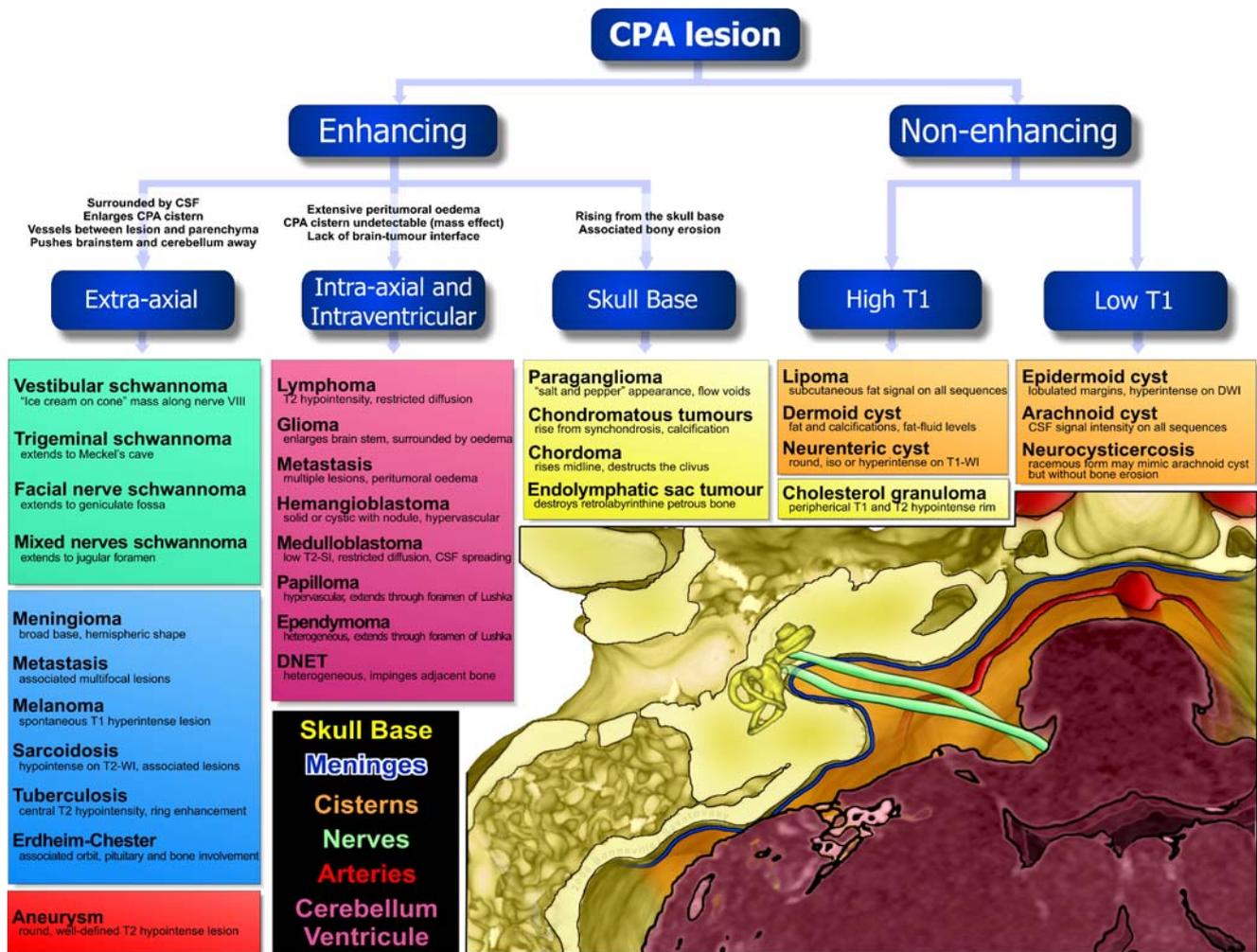


**Fig. 1** Drawing of a segmental approach to diagnosis of CPA lesions based on gadolinium enhancement, site of origin and key feature (adapted from reference [1], with permission)

isodense and enhance after contrast administration. On MRI, they show T1 isointensity and T2 high signal intensity, but appear as a hypointense filling defect on T2-weighted high-resolution MR cisternography, and enhance strongly after gadolinium injection. Enhancement of the adjacent meninges is possible in vestibular schwannoma and is not specific to meningiomas [4]. Three different MRI appearances of the tumoral enhancement are described in vestibular schwannomas: homogeneous (50–60%), heterogeneous (30–40%), and cystic (5–15%) [5–7]. The size of vestibular schwannomas is correlated to the appearance of the signal and the gadolinium uptake, and the histological Antoni subtype: small vestibular schwannomas are usually homogeneous and histologically composed of Antoni type A pattern, while heterogeneous and cystic vestibular schwannomas are larger and harbour Antoni B pattern or a mix of type A and B [7]. It is noteworthy that vestibular schwannomas always become heterogeneous in lesions larger than 25 mm in diameter because of the occurrence of those additional cystic or necrotic components (Fig. 2) [8]. Aside from the classic IAC-CPA schwannomas, small, purely intracanalicular schwannomas exist, but may also present with a dumbbell extension in the cochlea or vestibule [9]. In contrast, purely intracisternal vestibular schwannomas, exclusively located in the CPA without IAC involvement, represent a distinct entity because they have a large space to grow in before becoming symptomatic, thus leading to cerebellum, brain stem or fourth ventricle compression rather than hearing loss, and at imaging are always large, heterogeneous and may show hypervascularity with possible high flow vessels [10]. Differential diagnosis with other CPA lesions is not always simple and advanced techniques may solve difficult cases. On 3D fast spin-echo heavily T2-weighted sequence, a small focus of high signal T2 intensity observed in the dorsal brain stem on the same side of a CPA tumour presumably results from the degeneration of the vestibular nucleus associated with vestibular schwannoma and may therefore be suggestive of the diagnosis (Fig. 3) [11]. DWI shows the solid component of vestibular schwannomas to be usually isointense to the
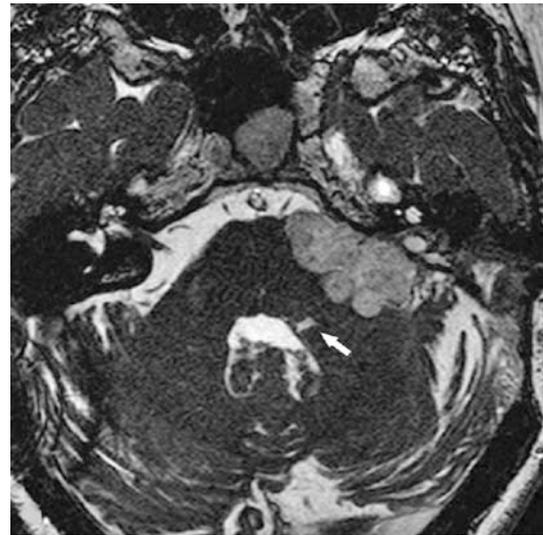


**Fig. 3** Post-therapeutic remnant of another large vestibular schwannoma in a 44-year-old woman. Axial infra-millimetric heavily T2-weighted image depicts a focus of high signal intensity in the dorsal brain stem (arrow), on the same side of the CPA tumour, presumed to result from the degeneration of the vestibular nucleus

normal parenchyma, with apparent diffusion coefficient (ADC) values ranging from 1.1 to $1.7 \times 10^{-3}$ mm$^2$/s in the literature and a raised mean ADC value compared to normal brain ($1.4 \times 10^{-3}$ mm$^2$/s) [12, 13] (Table 1). It has been postulated that higher ADC may reflect the lower cell density of Antoni type B schwannomas [13]. However, though the mean ADC value is significantly higher than in meningiomas [13], there is a great deal of overlap between them, so DWI does not reliably differentiate these two entities. On the other hand, the relative tumour blood volume [usually expressed as the relative cerebral blood volume (rCBV) in the literature, even for extra-axial lesions] evaluated with perfusion imaging is significantly lower in vestibular schwannomas than meningiomas [14]. Even if there is an overlap between the rCBV ratios of both entities (rCBV ratio = rCBV of the lesion/rCBV of the

**Fig. 2** Large vestibular schwannoma in a 53-year-old woman presenting with dizziness, left deafness and long-lasting headache. a. Contrast-enhanced axial T1-weighted image shows typical "ice cream-on-cone" CPA mass lesion that heterogeneously enhances. The component enlarging the porus of the internal auditory canal is very suggestive of the diagnosis. b. Short TE MR spectroscopy reveals a prominent peak of myo-inositol, another characteristic feature of schwannomas
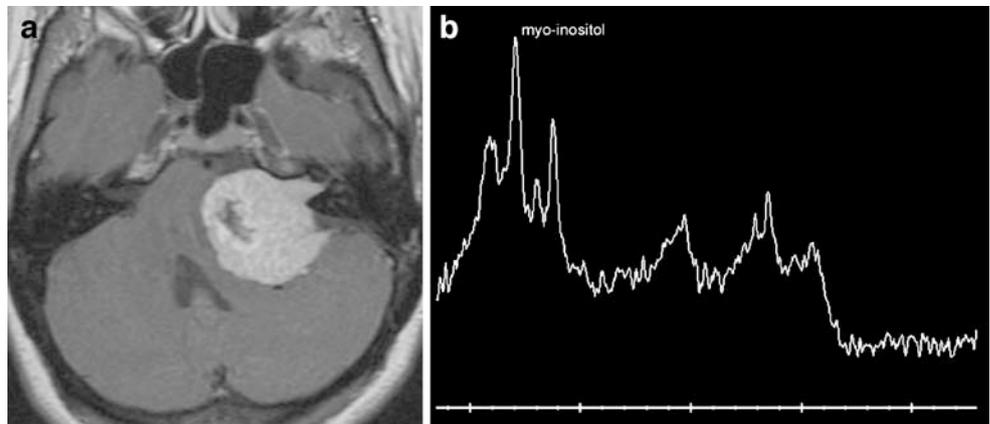
**Table 1** Summary of diffusion, perfusion and MR spectroscopy findings usually observed in the most frequent enhancing extra-axial cerebellopontine angle lesions

| Extra-axial lesions | DWI | ADC mean (min-max) | rCBV ratios mean (min-max) | Spectroscopy |
|---|---|---|---|---|
| Schwannoma | Isointense | 1.4 (1.1–1.7) | 3 (2.2–4.4) | Myo-Inositol |
| Meningioma | Variable* | 1 (0.7–2.6) | 8 (3–18) | Alanine |
| Metastasis | Hypo- to isointense (rarely hyperintense) | 1.1 (0.8–1.5) | 5 (1.3–15) | Lipids and choline |
| Tuberculoma | Variable* | 1 (0.4–2.64) | <1 | Lipids |

Note: DWI: signal intensity on diffusion-weighted imaging; ADC: apparent diffusion coefficient, values are $\times 10^{-3}$mm$^2$/s; rCBV ratios: relative cerebral blood volume ratios of the lesion to the normal brain; spectroscopy: characteristic metabolite peaks found at MR spectroscopy. * Variable: for these lesions, signal intensity on DWI widely ranges from hypo- to hyperintense with no dominating pattern.

normal contralateral white matter), a threshold of 4.4 is the highest rCBV ratio reported in schwannomas [14], while the mean rCBV ratio of typical meningiomas ranges from 6 to 9 [14–16].

Proton MR spectroscopy has rarely been reported in the work up of CPA lesions, certainly because of the frequent lipid contamination in spectra of extra-axial lesions abutting fatty bony limits of the posterior fossa. However, it seems interesting when feasible on large lesions, because it may help in distinguishing schwannomas from meningiomas by depicting a prominent myo-inositol peak in schwannomas at 3.55 ppm (Fig. 2), whereas alanine found in meningiomas is absent in schwannomas [17].

Once the diagnosis is made, MRI may be used to optimise treatment planning with respect to several features of the lesion: (i) the size of the tumour, which is assessed most reproducibly on high-resolution axial slices by measuring the two largest diameters of the extracanalicular portion of the tumour, parallel and perpendicular to the posterior surface of the petrous temporal bone [18]; (ii) the distance between the lateral extremity of the intracanalicular portion of the tumour and the fundus because it affects the hearing prognosis and may modify the surgical approach. This is better demonstrated with the heavily T2-weighed MR cisternography as it clearly depicts the lesion as hypointense within the high-signal of the CSF [19]; (iii) the intralabyrinthine signal intensity: while normal labyrinthine signal intensities are hyperintense on 3D fast spin-echo T2-weighted images and suppressed on fluid attenuated inversion recovery (FLAIR) sequence, poor hearing prognosis may be predicted by a low T2-signal intensity of labyrinth contents compared to the unaffected ear [20], which probably corresponds to a weakly suppressed signal intensity on FLAIR sequence; (iv) the identification of the facial nerve and its position relative to the vestibular schwannoma. This is sometimes demonstrated by the use of heavily 3D T2-weighted sequence [21], but is almost certainly better depicted by the administration of contrast material that amplifies the difference of signal intensities between the lesion and the facial nerve.
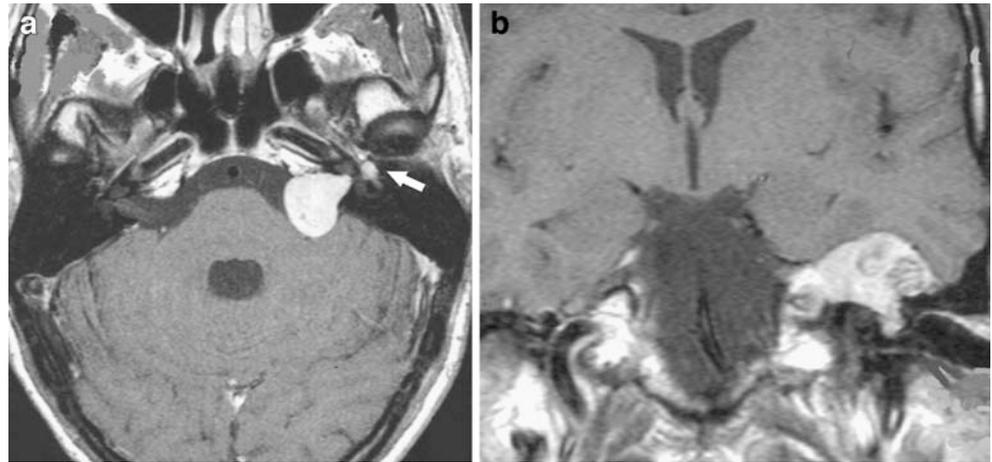
*Other cranial nerve schwannomas*

Non-vestibular schwannomas are rarely present in the CPA [1]. If signal intensities and post-contrast behaviours are similar to those of vestibular schwannomas, they are easily distinguished from them because they present with different symptoms, neuroanatomic locations, shapes and relationships with skull base foramina and canals. Trigeminal schwannoma is the most frequent lesion among non-vestibular schwannomas. It is located cephalad to vestibular schwannoma, has an anterior-posterior direction in the CPA cistern and may extend into Meckel's cave and along the trigeminal branches. Facial nerve schwannomas involving CPA/IAC may be difficult to distinguish from vestibular schwannomas because of their similar anatomical location and clinical presentation. However, they usually have a dumbbell shape with an extension along the different segments of the nerve into the temporal bone, as well as a suggestive associated round mass projecting up into the middle cranial fossa due to a component developing at the geniculate fossa (Fig. 4) [22]. Finally, glossopharyngeal, vagus and spinal accessory nerves schwannomas, also called jugular foramen schwannomas, may extend cranially with a large component coming back up in the CPA, especially when cystic, and mimic an intracisternal vestibular schwannoma (Fig. 5). However, a more caudal centre and the extension through an enlarged jugular foramen are the key features of the diagnosis [23].

*Meningioma*

Meningioma is the most common intracranial extra-axial tumour in adults, but is the second most frequent lesion in the CPA after vestibular schwannoma, representing 10%–15% of all tumours in this location [2]. Meningiomas arise from arachnoid meningothelial cells and grow slowly in the CPA, independently from the internal auditory canal. They are usually located at the posterior aspect of the temporal bone or at the premeatal area, from where they can easily extend into the IAC, but without enlarging the porus (Fig. 6) [24, 25]. At CT, meningiomas are hyperdense in 70% of the cases, calcified in about 20% and show a

**Fig. 4** Left facial nerve schwannoma in a 47-year-old man presenting with left facial palsy, sensorineural hearing loss and tinnitus. a. Contrast-enhanced axial T1-weighted image demonstrates a CPA mass mimicking a common vestibular schwannoma, except for the intralabyrinthine enhancing component (arrow). b. Contrast-enhanced coronal T1-weighted image shows a large infratemporal tumoral component, located at the geniculate fossa, a feature suggestive of a facial schwannoma



frequent adjacent bone reaction including hyperostosis and enostotic spur [25]. MRI clearly depicts a broad-based dural hemispheric or oval lesion, attached to the petrous dura mater or the inferior aspect of the tentorium. Meningiomas are usually isointense with the cortex on all sequences, and strongly enhance after contrast injection, often homogeneously. Though not specific to meningiomas [4], the intense enhancement of the non-neoplastic thickened peritumoral dura, the so-called "dural tail sign", is particularly frequent in association with meningiomas and should suggest the diagnosis when observed. This sign, and other conventional MR features, may look very similar in a wide variety of dural tumoral lesions in the CPA, including the different subtypes of meningiomas (meningothelial, fibrous, transitional, atypical, anaplastic or clear cell meningiomas [26]), solitary fibrous tumours [27], lymphomas [28, 29] or metastases [30], making preoperative differentiation difficult. The value of DWI is still questionable in the differential diagnosis and the pathological grading of meningiomas, but it seems that atypical or malignant meningiomas tend to have lower ADCs than the benign ones [31]. On the other hand, lymphomas have low ADCs as well. As previously mentioned, dynamic contrast-enhanced perfusion MR imaging finds very high mean rCBV ratios in meningiomas, ranging from 6 to 9, with even higher rCBV ratios in atypical meningiomas (Table 1) [14]. Interestingly, this is significantly higher than in schwannomas (mean rCBV ratio=3) or in lymphomas (mean rCBV ratio=1), thus providing another characteristic that allows discrimination between these CPA lesions [14]. At proton MR spectroscopy, the combination of elevated glutamate/glutamine and the characteristic presence of alanine at 1.5 ppm are considered very specific for meningiomas (Fig. 6) [17]. Three-dimensional high-resolution T2-weighted sequence should also be performed in the work up of CPA meningiomas because the neurosurgical outcome depends not only on their consistency and size, but also on their precise location and relation to the surrounding neurovascular structures [32]. Similarly, the extent of the involvement of the IAC should be assessed by this sequence
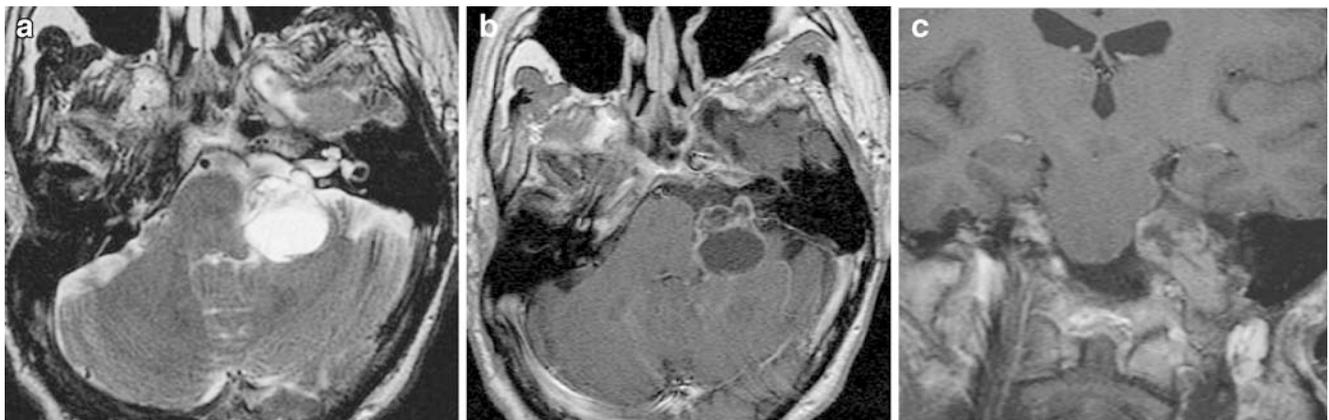


**Fig. 5** Jugular foramen schwannoma in a 38-year-old woman. a. Axial T2-weighted image and (b) gadolinium-enhanced axial T1-weighted image show a cystic lesion exactly located in front of the IAC. c. Contrast-enhanced coronal T1-weighted image reveals the extent of the schwannoma along the course of the mixed nerves, towards the jugular foramen
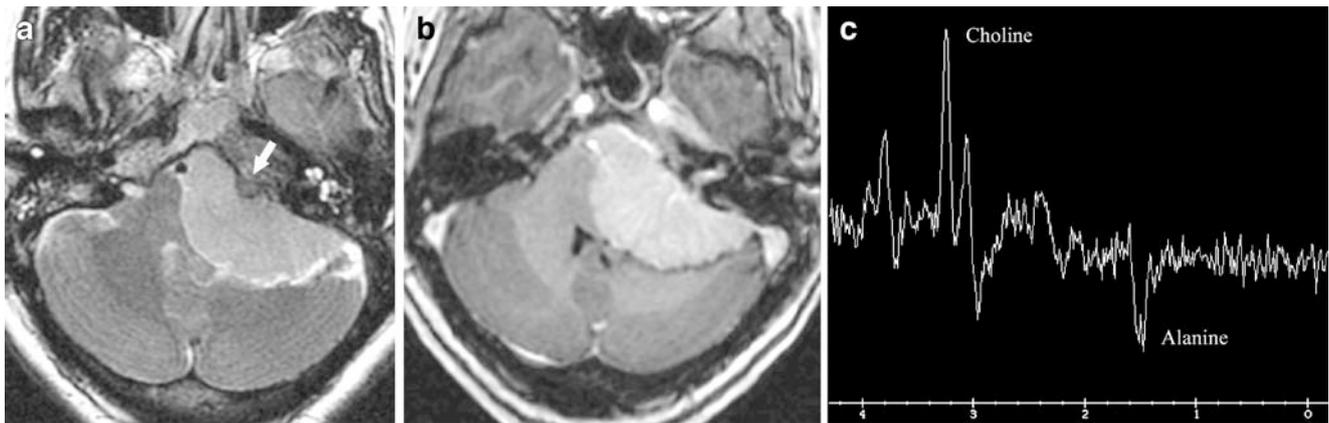
**Fig. 6** Left CPA meningioma in a 49-year-old woman with dizziness and left sensorineural hearing loss. a. Axial T2-weighted image reveals an homogeneous extra-axial hyperintense mass compressing the brain stem and the anterior aspect of the left cerebellar hemisphere away. Note the enostotic spur at the premeatal area (arrow), a feature suggestive of a meningioma. b. Contrast-enhanced axial gradient echo T1-weighted image shows an intense enhancing lesion with even an extension within the IAC. c. Proton MR spectroscopy, at long TE=135 ms, shows the characteristic presence of a negative doublet of alanine observed at 1.5 ppm

because surgery of meningiomas in the CPA involving the IAC carries an increased rate of cranial nerve morbidity and should therefore require special surgical management [33].

*Metastases*

Meningeal metastases from lung or breast cancers, melanoma (see below), or more rarely from other cancers, may invade the CPA. If CPA metastases should be sought when vertigo or other cranial nerve symptoms appear in a known cancer patient [34], however, correct preoperative diagnosis is frequently difficult in patients in whom a primary tumour has not been detected at the time of identification of the lesion in the CPA. At imaging, the presence of multifocal cerebral lesions is highly suggestive of metastases (Fig. 7), but CPA metastases may be solitary and mimic benign tumours of the CPA [30, 35], or be bilateral, mimicking neurofibromatosis 2 [36]. Metastases from cutaneous melanomas certainly represent the most frequent aetiology of melanocytic tumours in the CPA [37]. However, the few melanocytes normally present in the meninges of the posterior fossa may uncommonly give rise to benign or malignant primary melanocytic tumours [1, 38]. An epidermoid cyst associated with malignant melanocytic cells has also been the subject of a single case report of an unusual pigmented tumour in the CPA [39]. Final diagnosis is usually made by pathological analysis of a dural lesion resembling meningioma at preoperative imaging [1, 38]. The pigmented nature of this meningioma-like mass could, however, be suspected if it demonstrates subtle intrinsic homogeneous T1 high-signal intensity, due to the paramagnetic effect of the melanin contained in the tumour [1]. But except for melanocytic tumours, no imaging characteristic is pathognomonic of the diagnosis of metastases, but the unusual aggressiveness of an otherwise benign-

appearing mass resembling schwannoma or meningioma should make radiologists think of the possibility of a metastasis and examine the lungs and breast carefully [1]. On the other hand, perfusion MR imaging can provide additional information helpful in distinguishing dural metastases from meningiomas, by demonstrating rCBV ratios usually moderately elevated (often between 1.5 and 5), which may suggest the diagnosis of metastasis, while meningiomas have higher rCBV ratios (around 8) [15], and lymphomas rCBV almost equal to that of the normal parenchyma (see part II of this work for more
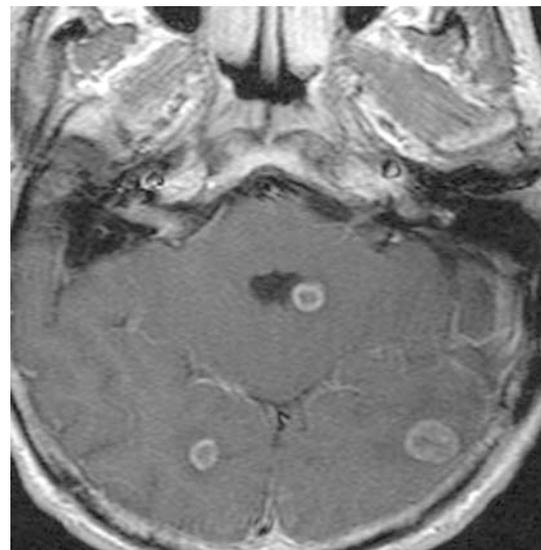


**Fig. 7** Intra- and extra-axial metastases in a 69-year-old man with lung cancer and intracranial hypertension syndrome. Contrast-enhanced axial T1-weighted image demonstrates a right IAC-CPA lesion that may mimic a small vestibular schwannoma. The combination with multiple intra-axial lesions is suggestive of a metastasis
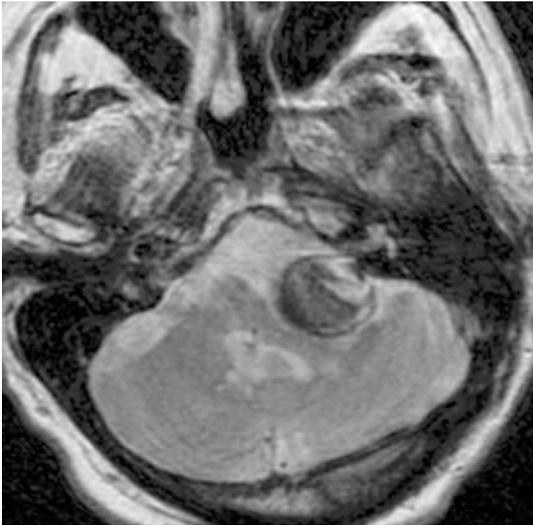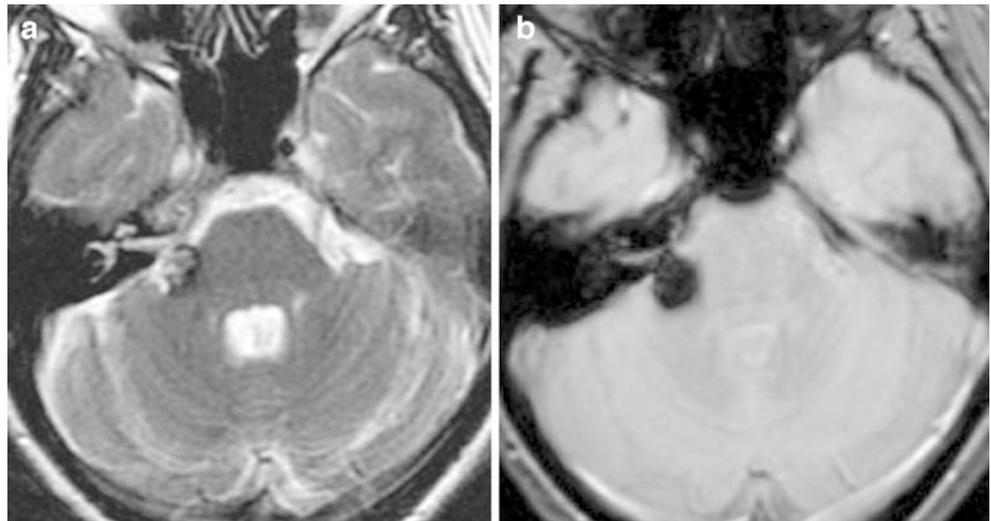
**Fig. 8** Partially thrombosed giant vertebrobasilar aneurysm in a 76-year-old man with vascular dementia. Axial T2-weighted image demonstrates a well-defined round hypointense lesion, very suggestive of an aneurysm, that was subsequently confirmed by an MR angiogram (not shown)

*Aneurysm*

Vertebrobasilar aneurysms and dolichoectasia account for a substantial part of non-tumoral lesions of the CPA that can lead to cranial nerves or brain stem compression [41]. In this location, and even in the internal auditory canal, intracranial aneurysms may resemble vestibular schwannomas, especially on CT, because they appear as well-defined round or oval lesions that intensely enhance after contrast administration [42]. At MRI, aneurysms without significant internal thrombus have obvious flow voids and pulsation artefacts on all spin echo sequences, but demonstrate iso— to high signal intensities and variable patterns of gadolinium uptake on T1-weighted images when intraluminal thrombus is present. However, the diagnosis should systematically be suspected when round/oval lesions with low to no signal intensity are seen on T2-weighted sequence (Fig. 8) [1]. MR angiography should then be performed to confirm the diagnosis and depict the parent artery, which could be the postero-inferior cerebellar artery [1], the antero-inferior cerebellar artery [43], the vertebral artery [44] or the basilar artery itself.

details on lymphomas). On DWI, the majority of necrotic metastatic lesions will have elevated diffusivity with low signal and high ADC values [13]. Exceptions are adenocarcinoma metastases that may mimic abscesses with restricted diffusivity and high signal on DWI and low ADC values. MR spectroscopy shows, in addition to elevated choline, a predominant peak of lipids in metastases, another important finding considered suggestive of the diagnosis [40].

*Cavernoma*

Cavernous malformations can also be encountered in the CPA. Even if most infratentorial cavernomas are located in the pons, superficial intra-axial cerebellar or even extra-axial cavernomas in the CPA exist and may clinically and radiologically mimic vestibular schwannomas [45]. MRI accurately establishes the diagnosis in most cases of intra-axial cavernomas: they appear as well-circumscribed lesions with a reticulated core of mixed signal intensity on T1-weighted images and usually high signal intensity on T2-weighted images, surrounded by a peripheral rim of hemosiderin that shows hypointensity on all sequences,

**Fig. 9** Right CPA cavernoma in a 42-year-old woman with headache. a. Axial T2-weighted image reveals a typical "pop-corn" lesion in front of the right IAC, with a hyperintense core surrounded by a peripheral rim of low signal intensity. b. Gradient echo T2-weighted image at the same level highlights the hemorrhagic nature of the lesion
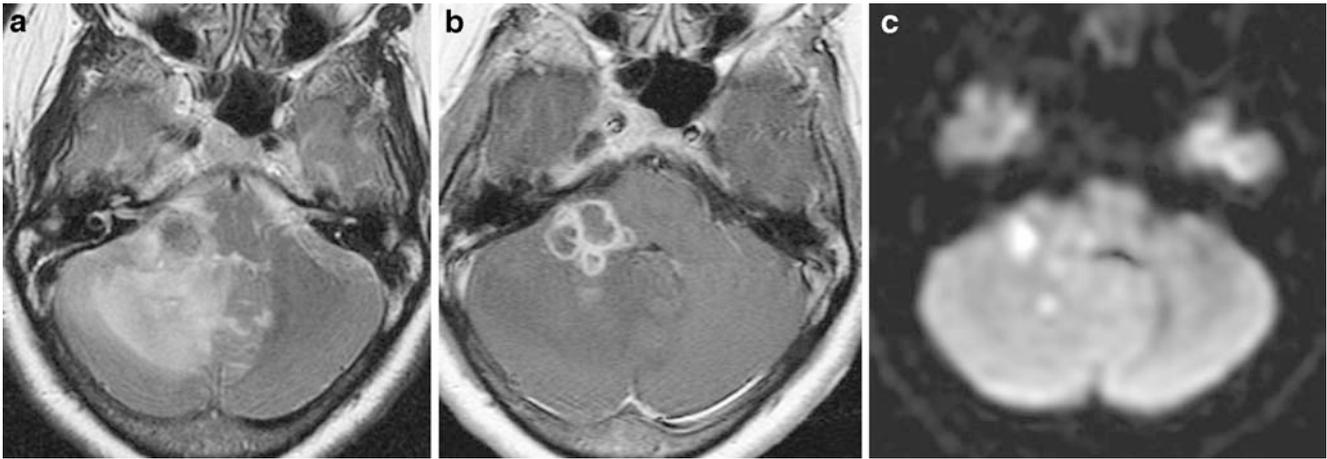
**Fig. 10** Tuberculomas in a 31-year-old woman with meningitis and right cerebellar syndrome. a. Axial T2-weighted image reveals, in front of the right IAC, several cerebellar superficial lesions with a mixture of iso- and hyposignal intensities. b. Contrast-enhanced axial T1-weighted image shows peripheral rim enhancement of these gathered lesions c. Tuberculomas present with either iso- or hypersignal intensities on diffusion-weighted image, but apparent diffusion coefficients were always within normal values, similar to that of parenchyma

with moderate to no enhancement after contrast injection (Fig. 9). Extra-axial CPA cavernomas are different and arise from the cranial nerves. Most of the reported cases had a faint intrinsic increased signal on T1-weighted images, with variable enhancement after gadolinium administration, and showed more classical central T2 hyperintensity surrounded by a rim of low signal intensity [46–48]. The presence of another or multiple intraparenchymal hypointense lesions detected by gradient echo T2-weighted images is a clue that points toward the diagnosis.

## Sarcoidosis

Sarcoidosis involves the nervous system in about 5% of the cases and usually manifests as a granulomatous inflammation of the meninges and the hypothalamic region. The meningeal lesions appear in a diffuse plaque-like pattern, but infrequent focal dural-based masses have occasionally been reported in the CPA [49–51]. Diagnosis is difficult, but can be considered because the sarcoidosis granulomas are hyperattenuating at CT, isointense on T1-weighted images, intensely enhance after contrast media injection and overall demonstrate a suggestive homogeneous low signal intensity on T2-weighted images [50].



**Fig. 11** Erdheim-Chester disease in a 38-year-old patient with diabetes insipidus and exophthalmia. a. Contrast-enhanced axial T1-weighted image reveals an extra-axial round mass in the left CPA that homogeneously enhances. b. Contrast-enhanced coronal T1-weighted image reveals an enhancing lesion at the stalk. c. Coronal T1-weighted image depicts identical lesions in both intra-conical spaces. The combination of granulomatous lesions in the meninges, the orbits and the sellar area is very suggestive of the diagnosis

## Tuberculosis

Central nervous system tuberculosis usually manifests as a tuberculous basilar meningitis that may be associated with intra-axial tuberculomas or tuberculous abscesses. Solitary tuberculoma presenting as an extra-axial mass mimicking a meningioma is, however, a classic but rare circumstance [52] that is even more uncommon in the CPA [53]. Superficial intraparenchymal tuberculomas, which are more frequent, may be difficult to distinguish from extra-axial lesions, and a high degree of suspicion for tuberculosis must be maintained when faced with a so-called CPA mass in the presence of risk factors for tuberculosis. CT and MR imaging findings vary depending on the stage of the disease and the character of the lesion (i.e., non-caseating, caseating with solid centre or caseating with necrotic centre) [54]. This may explain why cases of tuberculomas with no restricted diffusion and normal ADC have been reported [55]. Other cases that are caseating with a solid centre present as ring-enhancing lesions, with a central T2 hypointensity that parallels a high signal intensity on diffusion-weighted images and a possible low ADC [56]. The presence of multiple concomitant lesions with different DWI patterns may finally be a clue for the diagnosis of tuberculous lesions (Fig. 10). MR spectroscopy may also be helpful in reaching the diagnosis of tuberculoma: in a case report of a lesion located outside the posterior fossa, it distinguished an extra-axial tuberculoma from a meningioma by depicting elevated lipids peaks at 0.9 and 1.33 ppm and findings characteristic of tuberculomas [57]. Interestingly, these peaks detected in the lesion core of tuberculomas by proton MR spectroscopy also differed distinctively from those of the pyogenic brain abscesses [56]. Finally, and contrary to tumours, infectious lesions and especially tuberculomas demonstrate hypoperfusion on MR perfusion with rCBV ratios usually <1 [14].

## Erdheim-Chester disease

Erdheim-Chester disease is a rare systemic non-Langerhans histiocytosis of unknown aetiology that affects multiple organ systems, with a predilection for bones, orbits and brain. Cerebral involvement is caused by a mixed infiltrative pattern (widespread lesions, nodules or intracerebral masses of the dentate and pituitary regions) and extra-axial meningeal masses, with either thickening of the dura mater or meningioma-like tumours [58, 59]. Diagnosis of the extra-axial abnormality is challenging if the underlying disorder has not been identified, because the meningeal enhancing dural masses may resemble meningiomas [4]. However, the combination of dural lesions with intra-orbital and pituitary masses and osteosclerotic changes of the bones in a patient with a cerebellar syndrome is highly suggestive of the diagnosis (Fig. 11).

## Conclusion

A wide variety of lesions can be encountered in the CPA. A meticulous analysis of the site of origin, shape, density, signal intensities and behaviour after contrast media injection allows a systematic approach to the preoperative diagnosis in the majority of cases. Diffusion and perfusion-weighted imaging, as well as MR spectroscopy may also provide crucial information that helps radiologists arrive at the correct diagnosis non-invasively.

## References

1. Bonneville F, Sarrazin JL, Marsot-Dupuch K et al (2001) Unusual lesions of the cerebellopontine angle: a segmental approach. Radiographics 21:419–438
2. Sarrazin JL (2006) Infra tentorial tumors. J Radiol 87:748–763
3. Moffat DA, Ballagh RH (1995) Rare tumours of the cerebellopontine angle. Clin Oncol (R Coll Radiol) 7:28–41
4. Guermazi A, Lafitte F, Miaux Y et al (2005) The dural tail sign-beyond meningioma. Clin Radiol 60:171–188
5. Charabi S, Tos M, Thomsen J et al (2000) Cystic vestibular schwannoma-clinical and experimental studies. Acta Otolaryngol Suppl 543:11–13
6. Delsanti C, Regis J (2004) Cystic vestibular schwannomas. Neurochirurgie 50:401–406
7. Gomez-Brouchet A, Delisle MB, Cognard C et al (2001) Vestibular schwannomas: correlations between magnetic resonance imaging and histopathologic appearance. Otol Neurotol 22:79–86
8. Duvoisin B, Fernandes J, Doyon D et al (1991) Magnetic resonance findings in 92 acoustic neuromas. Eur J Radiol 13:96–102
9. Salzman KL, Davidson HC, Harnsberger HR et al (2001) Dumbbell schwannomas of the internal auditory canal. AJNR Am J Neuroradiol 22:1368–1376
10. Bonneville F, Cattin F, Czorny A, Bonneville JF (2002) Hypervascular intracisternal acoustic neuroma. J Neuroradiol 29:128–131
11. Okamoto K, Furusawa T, Ishikawa K, Sasai K, Tokiguchi S (2006) Focal T2 hyperintensity in the dorsal brain stem in patients with vestibular schwannoma. AJNR Am J Neuroradiol 27:1307–1311
12. Sener RN (2003) Diffusion magnetic resonance imaging of solid vestibular schwannomas. J Comput Assist Tomogr 27:249–252
13. Yamasaki F, Kurisu K, Satoh K et al (2005) Apparent diffusion coefficient of human brain tumors at MR imaging. Radiology 235:985–991
14. Hakyemez B, Erdogan C, Bolca N et al (2006) Evaluation of different cerebral mass lesions by perfusion-weighted MR imaging. J Magn Reson Imaging 24:817–824

15. Kremer S, Grand S, Remy C et al (2004) Contribution of dynamic contrast MR imaging to the differentiation between dural metastasis and meningioma. Neuroradiology 46:642–648
16. Yang S, Law M, Zagzag D et al (2003) Dynamic contrast-enhanced perfusion MR imaging measurements of endothelial permeability: differentiation between atypical and typical meningiomas. AJNR Am J Neuroradiol 24:1554–1559
17. Cho YD, Choi GH, Lee SP, Kim JK (2003) (1)H-MRS metabolic patterns for distinguishing between meningiomas and other brain tumors. Magn Reson Imaging 21:663–672
18. Walsh RM, Bath AP, Bance ML, Keller A, Rutka JA (2000) Comparison of two radiologic methods for measuring the size and growth rate of extracanalicular vestibular schwannomas. Am J Otol 21:716–721
19. Kocaoglu M, Bulakbasi N, Ucoz T et al (2003) Comparison of contrast-enhanced T1-weighted and 3D constructive interference in steady state images for predicting outcome after hearing-preservation surgery for vestibular schwannoma. Neuroradiology 45:476–481
20. Somers T, Casselman J, de Ceulaer G, Govaerts P, Offeciers E (2001) Prognostic value of magnetic resonance imaging findings in hearing preservation surgery for vestibular schwannoma. Otol Neurotol 22:87–94
21. Sartoretti-Schefer S, Kollias S, Valavanis A (2000) Spatial relationship between vestibular schwannoma and facial nerve on three-dimensional T2-weighted fast spin-echo MR images. AJNR Am J Neuroradiol 21:810–816
22. Wiggins RH, 3rd, Harnsberger HR, Salzman KL et al (2006) The many faces of facial nerve schwannoma. AJNR Am J Neuroradiol 27:694–699
23. Wilson MA, Hillman TA, Wiggins RH, Shelton C (2005) Jugular foramen schwannomas: diagnosis, management, and outcomes. Laryngoscope 115:1486–1492
24. Le Garlantezec C, Vidal VF, Guerin J et al (2005) Management of cerebellopontine angle meningiomas and the posterior part of the temporal bone. Report on 44 cases. Rev Laryngol Otol Rhinol (Bord) 126:81–89
25. Helie O, Soulie D, Sarrazin JL et al (1995) Magnetic resonance imaging and meningiomas of the posterior cerebral fossa. 31 cases. J Neuroradiol 22:252–270
26. Yu KB, Lim MK, Kim HJ et al (2002) Clear-cell meningioma: CT and MR imaging findings in two cases involving the spinal canal and cerebellopontine angle. Korean J Radiol 3:125–129
27. Bikmaz K, Cosar M, Kurtkaya-Yapicier O, Iplikcioglu AC, Gokduman CA (2005) Recurrent solitary fibrous tumour in the cerebellopontine angle. J Clin Neurosci 12:829–832
28. Kawamura S, Yamada M, Nonoyama Y et al (1998) Intrameatal tumours presenting as a hearing disturbance: case reports of meningioma and lymphoma. Acta Neurochir (Wien) 140:675–679
29. Cotton F, Ongolo-Zogo P, Louis-Tisserand G et al (2006) Diffusion and perfusion MR imaging in cerebral lymphomas. J Neuroradiol 33:220–228
30. Buis DR, Peerdeman SM, Vandertop WP (2004) Metastatic adenocarcinoma in the cerebellopontine angle, presenting as a meningioma: a case report of rare occurrence. Acta Neurochir (Wien) 146:1369–1372; discussion 1372
31. Filippi CG, Edgar MA, Ulug AM et al (2001) Appearance of meningiomas on diffusion-weighted images: correlating diffusion constants with histopathologic findings. AJNR Am J Neuroradiol 22:65–72
32. Gerganov V, Bussarsky V, Romansky K et al (2003) Cerebellopontine angle meningiomas. Clinical features and surgical treatment. J Neurosurg Sci 47:129–135; discussion 135
33. Roser F, Nakamura M, Dormiani M et al (2005) Meningiomas of the cerebellopontine angle with extension into the internal auditory canal. J Neurosurg 102:17–23
34. Lin ZM, Young YH (2005) Investigating the causes of vertigo in breast cancer survivors. Eur Arch Otorhinolaryngol 262:432–436
35. Yuh WT, Mayr-Yuh NA, Koci TM et al (1993) Metastatic lesions involving the cerebellopontine angle. AJNR Am J Neuroradiol 14:99–106
36. Hariharan S, Zhu J, Nadkarni MA, Donahue JE (2005) Metastatic lung cancer in the cerebellopontine angles mimicking bilateral acoustic neuroma. J Clin Neurosci 12:184–186
37. Shinogami M, Yamasoba T, Sasaki T (1998) Bilateral isolated metastases of malignant melanoma to the cerebellopontine angle. Otolaryngol Head Neck Surg 118:276–279
38. Kan P, Shelton C, Townsend J, Jensen R (2003) Primary malignant cerebellopontine angle melanoma presenting as a presumed meningioma: case report and review of the literature. Skull Base 13:159–166
39. Meng FG, Wu CY, Liu ZH, Zhu SG, Liu YG (2006) Epidermoid cyst with infiltrative malignant melanoma in the cerebellopontine angle. J Clin Neurosci 13:669–672
40. Bulakbasi N, Kocaoglu M, Ors F, Tayfun C, Ucoz T (2003) Combination of single-voxel proton MR spectroscopy and apparent diffusion coefficient calculation in the evaluation of common brain tumors. AJNR Am J Neuroradiol 24:225–233
41. Papanagiotou P, Grunwald IQ, Politi M et al (2006) Vascular anomalies of the cerebellopontine angle. Radiologe 46:216–223
42. DiMaio S, Mohr G, Dufour JJ, Albrecht S (2003) Distal mycotic aneurysm of the AICA mimicking intracanalicular acoustic neuroma. Can J Neurol Sci 30:388–392
43. Sarkar A, Link MJ (2004) Distal anterior inferior cerebellar artery aneurysm masquerading as a cerebellopontine angle tumor: case report and review of literature. Skull Base 14:101–106; discussion 106–107
44. Monksfield P, Martinez Devesa P, Molyneux A, Milford C (2005) Vertebral artery aneurysm causing contralateral cerebellopontine angle mass effect. Otol Neurotol 26:525–527
45. Beskonakli E, Kaptanoglu E, Okutan O, Solaroglu I, Taskin Y (2002) Extra-axial cavernomas of the cerebellopontine angle involving the seventh-eighth nerve complex. Neurosurg Rev 25:222–224
46. Ferrante L, Acqui M, Trillo G et al (1998) Cavernous angioma of the VIIIth cranial nerve. A case report. Neurosurg Rev 21:270–276
47. Cotton CA, Beall DP, Winter BJ et al (2006) Cavernous angioma of the cerebellopontine angle. Curr Probl Diagn Radiol 35:120–123
48. Deshmukh VR, Albuquerque FC, Zabramski JM, Spetzler RF (2003) Surgical management of cavernous malformations involving the cranial nerves. Neurosurgery 53:352–357; discussion 357
49. Sugisaki K, Miyazaki E, Fukami T et al (2000) A case of sarcoidosis presenting as multiple pulmonary nodules, nasopharyngeal and cerebellopontine tumors. Sarcoidosis Vasc Diffuse Lung Dis 17:82–85
50. Lipper MH, Goldstein JM (1998) Neurosarcoidosis mimicking a cerebellopontine angle meningioma. AJR Am J Roentgenol 171:275–276

51. Wani MK, Ruckenstein MJ, Robertson JH, Schweitzer JB (1999) Neurosarcoidosis: an unusual case presenting as a cerebellopontine angle tumor. Otolaryngol Head Neck Surg 121:301–302

52. Yanardag H, Uygun S, Yumuk V, Caner M, Canbaz B (2005) Cerebral tuberculosis mimicking intracranial tumour. Singapore Med J 46:731–733

53. Sathyanarayana S, Baskaya MK, Fowler M, Roberts R, Nanda A (2003) Solitary tuberculoma of the cerebellopontine angle: a rare presentation. J Clin Neurosci 10:120–122

54. Harisinghani MG, McLoud TC, Shepard JA et al (2000) Tuberculosis from head to toe. Radiographics 20:449–470; quiz 528–449, 532

55. Batra A, Tripathi RP (2004) Diffusion-weighted magnetic resonance imaging and magnetic resonance spectroscopy in the evaluation of focal cerebral tubercular lesions. Acta Radiol 45:679–688

56. Kaminogo M, Ishimaru H, Morikawa M, Suzuki Y, Shibata S (2002) Proton MR spectroscopy and diffusion-weighted MR imaging for the diagnosis of intracranial tuberculomas. Report of two cases. Neurol Res 24:537–543

57. Khanna PC, Godinho S, Patkar DP, Pungavkar SA, Lawande MA (2006) MR spectroscopy-aided differentiation: "giant" extra-axial tuberculoma masquerading as meningioma. AJNR Am J Neuroradiol 27:1438–1440

58. Weidauer S, von Stuckrad-Barre S, Dettmann E, Zanella FE, Lanfermann H (2003) Cerebral Erdheim-Chester disease: case report and review of the literature. Neuroradiology 45:241–245

59. Lachenal F, Cotton F, Desmurs-Clavel H et al (2006) Neurological manifestations and neuroradiological presentation of Erdheim-Chester disease: report of six cases and systematic review of the literature. J Neurol 253:1267–1277